iScience

CellPress
OPEN ACCESS

Article

Integrative neurovascular coupling and neurotransmitter analyses in anisometropic and visual deprivation amblyopia children

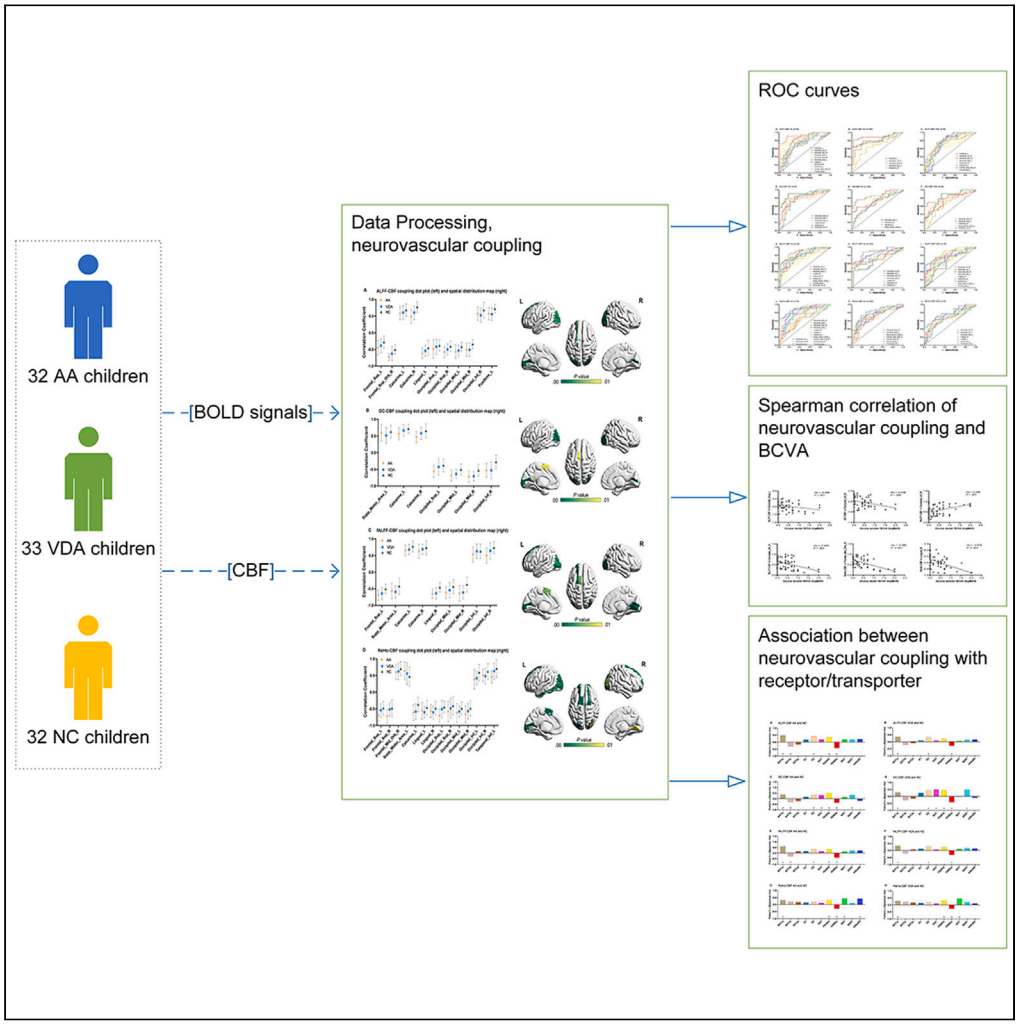

Xiaopan Zhang, Liang Liu, Yadong Li, ..., Guangying Zheng, Jingliang Cheng, Baohong Wen

109496417@qq.com (Y.Z.)
fccwenbh@zzu.edu.cn (B.W.)

Highlights

Neurovascular coupling dysfunction was observed in AA and VDA amblyopia children

Negative correlation was observed between ALFF-CBF coupling in Occipital_Sup and BCVA

Neurovascular coupling effect was associated with receptors/transporters in amblyopia

Zhang et al., iScience 27, 109988
June 21, 2024
https://doi.org/10.1016/j.isci.2024.109988

iScience

CellPress
OPEN ACCESS

Article

Integrative neurovascular coupling and neurotransmitter analyses in anisometropic and visual deprivation amblyopia children

Xiaopan Zhang,[1,4] Liang Liu,[1,4] Yadong Li,[2] Xiao Li,[2] Kejia Wang,[2] Shaoqiang Han,[1] Mengzhu Wang,[3] Yong Zhang,[1,*] Guangying Zheng,[2] Jingliang Cheng,[1] and Baohong Wen[1,5,*]

SUMMARY

The association between visual abnormalities and impairments in cerebral blood flow and brain region potentially results in neural dysfunction of amblyopia. Nevertheless, the differences in the complex mechanisms of brain neural network coupling and its relationship with neurotransmitters remain unclear. Here, the neurovascular coupling mechanism and neurotransmitter activity in children with anisometropic amblyopia (AA) and visual deprivation amblyopia (VDA) was explored. The neurovascular coupling of 17 brain regions in amblyopia children was significantly abnormal than in normal controls. The classification abilities of coupling units in brain regions differed between two types of amblyopia. Correlations between different coupling effects and neurotransmitters were different. The findings of this study demonstrate a correlation between the neurovascular coupling and neurotransmitter in children with AA and VDA, implying their impaired neurovascular coupling function and potential molecular underpinnings. The neuroimaging evidence revealed herein offers potential for the development of neural therapies for amblyopia.

INTRODUCTION

The association between visual abnormalities and impairments in cerebral blood flow and brain region functionality has been demonstrated, potentially resulting in neurophysiological changes.[1,2] Enhanced blood flow reduction in the primary visual cortex has been reported in patients with visual deprivation amblyopia (VDA), while decreased glucose metabolism has been observed in the primary visual cortex of patients with anisometropic amblyopia (AA).[3,4] Neurophysiological and histopathological abnormalities have been found to occur in the lateral geniculate nucleus and visual cortical area V1 of amblyopic eyes, but a reduction in the activation of extrastriate areas in AA children.[5,6] Studies have shown that AA and VDA exhibit diverse neuropathological molecular characteristics.[7,8] Studies have shown that amblyopia is related to protein metabolism in neural networks and extracellular matrix of visual cortex.[9,10] Dysfunction of synapses is a cause of visual impairment in AA and VDA;[11,12] the brain, by releasing stress hormones influence vascular tone, particularly in and around the optic nerve and thereby impair vascular autoregulation and neural metabolism.[13] These studies suggest that exploring brain neural coupling and its relationship with neurotransmitters is important for AA and the mechanisms of neurophysiological alterations in the VDA.

An increasing body of research suggests that neurons and blood flow form a functionally intertwined complex, allowing for a deeper understanding of the intricate physiological characteristics of brain activity.[14,15] Cerebral blood flow (CBF) derived from arterial spin labeling (ASL) signals is a non-invasive and reliable indicator.[16,17] Assessment of spontaneous neuronal activity using blood-oxygen-level-dependent (BOLD) signals represents a useful degree centrality (DC) map, while regional homogeneity (ReHo) maps, amplitude of low-frequency fluctuation (ALFF) maps, and fractional ALFF (fALFF) maps have been demonstrated as reliable evaluations of brain neural activity.[18–21] The evolution of neurovascular coupling measured by DC-CBF, ReHo-CBF, ALFF-CBF, and fALFF-CBF has become an effective means to describe the changes in brain neurovascular dynamics, as supported by previous studies.[22–24]

Here, an attempt is made to define the spatial correlation between CBF and BOLD signals on a regional basis to construct neurovascular coupling functional composite units. To achieve this, spatial correlation coefficients between CBF and DC, ReHo, ALFF, and fALFF at the brain region level are analyzed, and composite units are constructed based on this local relationship. As described further, it is demonstrated that there is a coupling relationship between neuronal activity and cerebral perfusion, which is associated with functional differences in physiological and pathological states between AA and VDA children.[25,26] Furthermore, integration of this complex unit with relationships to molecular and transcriptomic data is conducted, and differences in the neural mechanisms between AA and VDA are analyzed at multiple scales.

[1]Department of Magnetic Resonance Imaging, The First Affiliated Hospital of Zhengzhou University, Zhengzhou, China
[2]Department of Ophthalmology, The First Affiliated Hospital of Zhengzhou University, Zhengzhou, China
[3]MR Research Collaboration, Siemens Healthineers Ltd., Beijing, China
[4]These authors contributed equally
[5]Lead contact
*Correspondence: 109496417@qq.com (Y.Z.), fccwenbh@zzu.edu.cn (B.W.)
https://doi.org/10.1016/j.isci.2024.109988

Table 1. Demographic characteristics of participants

Conditions	AA	VDA	NC	*p* value
Male sex, no. (%)/Female sex, no. (%)	16 (50)/16 (50)	16 (48)/17 (52)	16 (50)/16 (50)	0.990[a]
Age, mean (SD), y	9.13 (2.65)	9.58 (2.91)	9.94 (2.14)	0.456[b]
OD visual acuity, median (IQR), logMAR	0.30 (0.02–0.70)	0.40 (0.05–0.91)	0.00 (0.00–0.00)	<0.001[c]
OS visual acuity, median (IQR), logMAR	0.56 (0.11–0.92)	0.52 (0.10–0.87)	0.00 (0.00–0.00)	<0.001[c]
OD BCVA, median (IQR), logMAR	0.19 (0.00–0.52)	0.30 (0.00–0.70)	0.00 (0.00–0.00)	<0.001[c]
OS BCVA, median (IQR), logMAR	0.40 (0.00–0.65)	0.40 (0.05–0.70)	0.00 (0.00–0.00)	<0.001[c]
OD diopter of spherical power, median (IQR), D	1.13 (0.00–2.44)	0.75 (−0.25 to 2.00)	0.00 (−0.19 to 1.00)	0.033[c]
OS diopter of spherical power, median (IQR), D	2.00 (0.13–6.06)	1.00 (−0.13 to 1.78)	0.00 (−0.19 to 0.73)	0.001[c]
OD diopter of cylindrical power, median (IQR), D	−0.25 (−1.69 to 0.75)	0.00 (−1.00 to 1.13)	0.00 (0.00–0.50)	0.446[c]
OS diopter of cylindrical power, median (IQR), D	−0.50 (−2.25 to 0.69)	0.00 (−1.00 to 0.88)	0.00 (0.00–0.50)	0.168[c]
OD intraocular pressure, mean (SD), mmHg	16.20 (3.86)	16.66 (4.43)	15.46 (2.41)	0.422[b]
OS intraocular pressure, mean (SD), mmHg	16.82 (3.77)	17.92 (6.22)	15.42 (2.47)	0.083[b]
OD amblyopia, no. (%)/OS amblyopia, no. (%)	16 (50)/16 (50)	17 (52)/16 (48)	N/A	N/A

OD, oculus dexter; OS, oculus sinister; AA, anisometropic amblyopia; VDA, visual deprivation amblyopia; NC, normal control; BCVA, best-corrected visual acuity; IQR, interquartile range; SD, standard deviation; logMAR, logarithm of the minimum angle of resolution; N/A, not applicable.

[a]Chi-square test.

[b]One-way analysis of variance.

[c]Kruskal-Wallis H test.

RESULTS

Clinical characteristics

Sixty-five children, with a mean (standard deviation [SD]) age of 9.35 (2.77) years, consisting of 32 males (49%) and 33 females (51%), were enrolled in the study, all diagnosed with amblyopia. They were stratified into two groups: AA (mean [SD] age = 9.13 [2.65], the age ranged from 6 to 15 years; 16 males [50%] and 16 females [50%]) and VDA (mean [SD] age = 9.58 [2.91], the age ranged from 6 to 16 years; 16 males [48%] and 17 females [52%]). Additionally, 32 individuals with normal vision (mean [SD] age = 9.94 [2.14], the age ranged from 5 to 14 years; 16 males [50%] and 16 females [50%]), referred to as normal controls (NC), were included in the study. There was no significant difference in gender; age; oculus dexter (OD), oculus sinister (OS) intraocular pressure; and OD, OS diopter of cylindrical power among the three groups. There were significant differences in the OD, OS visual acuity; OD, OS best-corrected visual acuity (BCVA); and OD, OS diopter of spherical power among the three groups (Table 1).

Functional composite units of neurovascular coupling and intergroup comparison results

Significant statistical differences were observed in 11 brain regions among the three groups of participants in the ALFF-CBF units (Figure 1A and Table S2). In the DC-CBF module, significant statistical differences were observed in three groups across seven brain regions (Figure 1B and Table S3). In the fALFF-CBF module, significant statistical differences were detected in three groups across nine brain regions (Figure 1C and Table S4). Statistically significant differences were observed in 14 brain regions among three groups within the ReHo-CBF units (Figure 1D and Table S5).

The receiver operating characteristic (ROC) curves were constructed to examine the ability of composite units in various brain regions to differentiate types of amblyopia. Detailed ROC results for all positive brain regions corresponding to composite units can be found in Table S6. There is good discriminative ability for all positive brain region indices between AA and NC and VDA and NC. In contrast, AA and VDA can only be differentiated through composite units in certain brain regions. All significant ROC distinctions are illustrated in Figure 2.

Correlation analysis results

The results of Spearman correlation analysis between neurovascular coupling changes in children with amblyopia and BCVA are depicted in Figure 3. Negative correlation was observed between ALFF-CBF coupling in the left superior occipital gyrus and OD BCVA ($rho = -0.499$; $p = 0.001$), as well as between DC-CBF coupling in the right inferior occipital gyrus and OS BCVA ($rho = -0.438$; $p = 0.006$). Additionally, a positive correlation was found between fALFF-CBF coupling in the right inferior occipital gyrus and OD BCVA ($rho = 0.489$; $p = 0.001$), while it exhibited a negative correlation with OS BCVA ($rho = -0.460$; $p = 0.003$). Moreover, ReHo-CBF coupling in the right middle frontal gyrus orbital part was negatively correlated with OD BCVA ($rho = -0.565$; $p < 0.001$). Similarly, ReHo-CBF coupling in the right lingual gyrus was negatively correlated with OS BCVA ($rho = -0.579$; $p < 0.001$).

The effect sizes of ALFF-CBF coupling between AA and NC were significantly correlated with the densities of 5 types of receptors/transporters, including 5HT1a, 5HT1b, D2, FDOPA, and GABAa (Figure 4A). The effect sizes of ALFF-CBF coupling between VDA and NC were

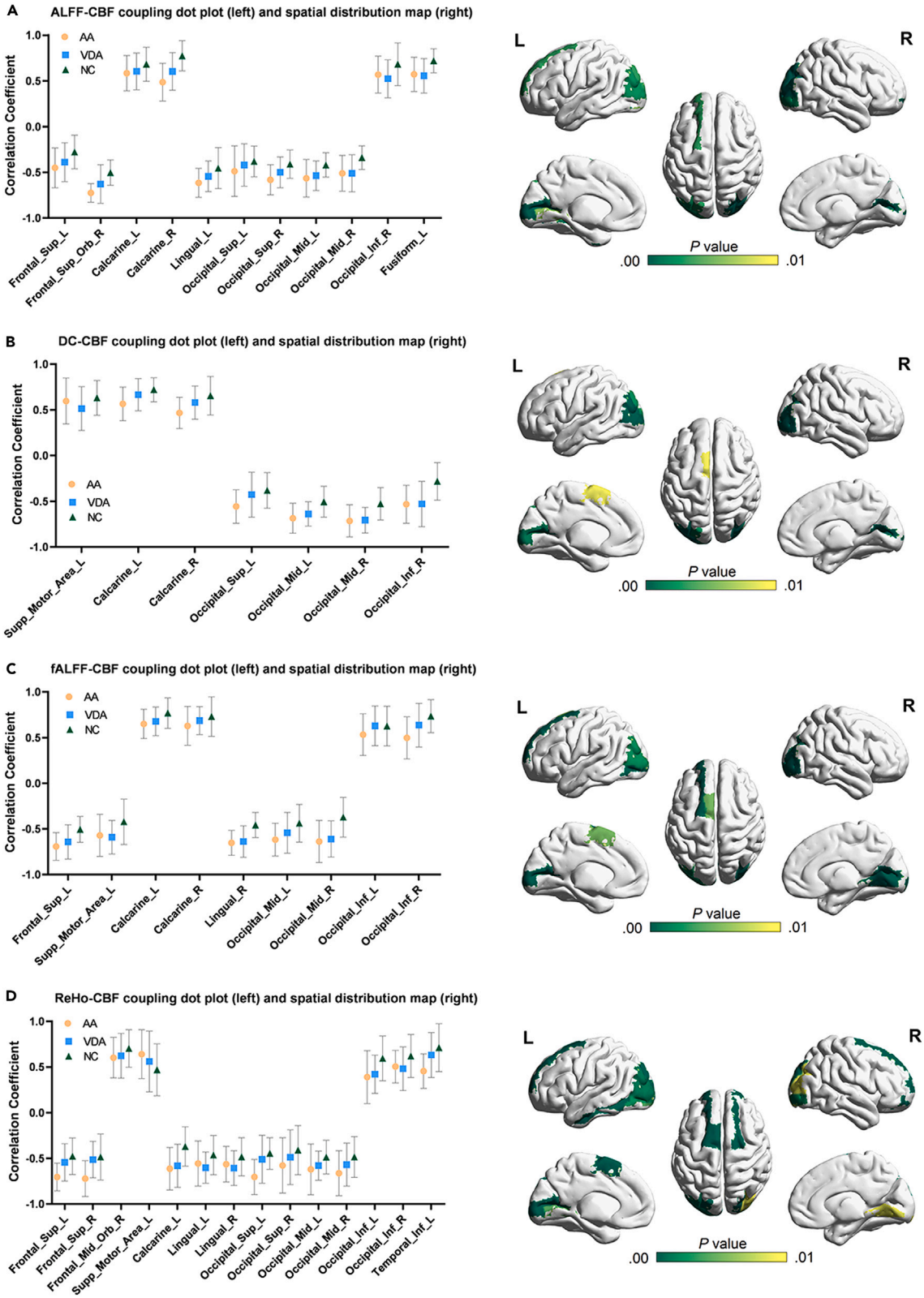
A
ALFF-CBF coupling dot plot (left) and spatial distribution map (right)
AA
VDA
NC
Correlation Coefficient
1.0
0.5
0.0
-0.5
-1.0
Frontal_Sup_L
Frontal_Sup_Orb_R
Calcarine_L
Calcarine_R
Lingual_L
Occipital_Sup_L
Occipital_Sup_R
Occipital_Mid_L
Occipital_Mid_R
Occipital_Inf_R
Fusiform_L
L
R
P value
.00
.01
B
DC-CBF coupling dot plot (left) and spatial distribution map (right)
AA
VDA
NC
Correlation Coefficient
1.0
0.5
0.0
-0.5
-1.0
Supp_Motor_Area_L
Calcarine_L
Calcarine_R
Occipital_Sup_L
Occipital_Mid_L
Occipital_Mid_R
Occipital_Inf_R
L
R
P value
.00
.01
C
fALFF-CBF coupling dot plot (left) and spatial distribution map (right)
AA
VDA
NC
Correlation Coefficient
1.0
0.5
0.0
-0.5
-1.0
Frontal_Sup_L
Supp_Motor_Area_L
Calcarine_L
Calcarine_R
Lingual_R
Occipital_Mid_L
Occipital_Mid_R
Occipital_Inf_L
Occipital_Inf_R
L
R
P value
.00
.01
D
ReHo-CBF coupling dot plot (left) and spatial distribution map (right)
AA
VDA
NC
Correlation Coefficient
1.0
0.5
0.0
-0.5
-1.0
Frontal_Sup_L
Frontal_Sup_R
Frontal_Mid_Orb_R
Supp_Motor_Area_L
Calcarine_L
Lingual_L
Lingual_R
Occipital_Sup_L
Occipital_Sup_R
Occipital_Mid_L
Occipital_Mid_R
Occipital_Inf_L
Occipital_Inf_R
Temporal_Inf_L
L
R
P value
.00
.01

Figure 1. The distribution of correlation coefficients and spatial distribution of their differences among four types of neurovascular coupling

(A–D) Dot plot and spatial distribution map of ALFF-CBF (A), DC-CBF (B), fALFF-CBF (C), and ReHo-CBF(D) coupling. The horizontal axis of the dot plot corresponds to brain region labels; orange dot represents AA, blue squares show VDA, and green triangles display NC. For details of the brain region label, see Table S1.

Abbreviations: ALFF-CBF, amplitude of low-frequency fluctuation-cerebral blood flow; DC-CBF, degree centrality-cerebral blood flow; fALFF-CBF, fractional amplitude of low-frequency fluctuation-cerebral blood flow; ReHo-CBF, regional homogeneity-cerebral blood flow; AA, anisometropic amblyopia; VDA, visual deprivation amblyopia; NC, normal control.

significantly correlated with the densities of 3 types of receptors/transporters, such as 5HT1a, D2, and GABAa (Figure 4B). The effect sizes of DC-CBF coupling between AA and NC were significantly correlated with 7 types of receptors/transporters (including 5HT1a, 5HT1b, D2, DAT, FDOPA, GABAa, and SERT) (Figure 4C). The effect sizes of DC-CBF coupling between VDA and NC were significantly correlated with 6 types of receptors/transporters, including 5HT1a, D2, DAT, FDOPA, GABAa, and SERT (Figure 4D). The effect sizes of fALFF-CBF coupling between AA and NC were significantly correlated with 5 types of receptors/transporters, comprising 5HT1a, 5HT1b, D2, FDOPA, and GABAa (Figure 4E). The effect sizes of fALFF-CBF coupling between VDA and NC were significantly correlated with 3 types of receptors/transporters, namely 5HT1a, D2, and GABAa (Figure 4F). The effect sizes of ReHo-CBF coupling between AA and NC were significantly correlated with 5 types of receptors/transporters, including 5HT1a, FDOPA, GABAa, noradrenaline transporter (NAT), and mGluR5 (Figure 4G). The effect sizes of ReHo-CBF coupling between VDA and NC were significantly correlated with 4 types of receptors/transporters, comprising 5HT1a, FDOPA, GABAa, and NAT (Figure 4H).

DISCUSSION

The multimodal neuroimaging mechanism underlying the intrinsic neuronal activity and corresponding cerebral blood perfusion in children with amblyopia was investigated in this study. Results revealed significant neurovascular coupling deficits in multiple brain regions among both AA and VDA children. Furthermore, distinct differences between various types of neurovascular coupling functional composite units were primarily concentrated in brain regions associated with visual mechanisms. Our findings further indicate that the impairment of neurovascular coupling in specific brain regions differs in its ability to differentiate between AA and VDA. The disparities in neurovascular coupling dysfunction between the two types of amblyopia were confirmed. The correlation between neurovascular coupling and the mechanism of amblyopia was emphasized, demonstrating an association between neurovascular coupling and BCVA. Finally, by demonstrating the association between the magnitude of neurovascular coupling effects in different types of amblyopia and receptor/transporter density, we highlight the potential molecular basis of neurovascular coupling dysfunction.

Previous studies have shown that there exists a close relationship at the cellular level between blood flow and neuronal function, typically resulting in the local cerebral arterial vasodilation through ion gradients in astrocytes and the metabolic activity of projecting neurons.[27] Surrounding neurons form networks around cell bodies and dendrites, regulating ion flow and conduction, which are associated with variations in local neural circuits coupled with blood transport.[28,29] Apart from cellular structural changes, macroscopic white matter development is also associated with local neural vascular coupling.[30] Changes in neurovascular coupling occur within the white matter of the brain, reflecting an enhancement in oligodendrocyte myelination.[31] Axons forming myelin support long-distance connections within the visual cortex;[32] similarly, neural impulses reduce the metabolic demands of neuronal cell bodies. Participation in the same BOLD signal pattern necessitates lower blood flow, consequently resulting in decreased neurovascular coupling.[33] Our study results indicate a significant abnormity in neurovascular coupling function in 17 brain regions among both types of amblyopic children compared to NC. These neurovascular coupling-deficient regions encompass most of the occipital lobe and a small portion of the frontal lobe, suggesting a mismatch between neuronal metabolic demand and blood oxygen supply in these brain regions of amblyopic children.[34]

Neurovascular coupling is considered an optimized high-fidelity system that reflects the interplay between nutritional demands and supply.[24] ALFF is defined as the total power within the low-frequency range, while fALFF is defined as the relative contribution of specific low-frequency fluctuations within detectable frequency ranges, reflecting the spontaneous neuronal activity of brain regions.[21,35] DC reflects the characteristics of the "hubs" within the brain's functional network, exhibiting high test-retest reliability and being capable of reflecting the corresponding blood supply and metabolism in central areas of the brain.[36] ReHo measures the functional consistency between specific voxels and their nearest neighbors, reflecting the synchronization level of local brain region neuronal emission, conduction, and metabolic activity.[37] Prior research has indicated that the coupling of ALFF-CBF, DC-CBF, fALFF-CBF, and ReHo-CBF can be understood as proxy variables for neurovascular coupling, providing a non-invasive window.[22–24,38] The coordinated brain activity in the associated networks of brain region distribution ensures a corresponding CBF in response to neural activities.[39] Dysfunction in neurovascular coupling reflects abnormal neural metabolic activity in the respective areas.[40,41] Based on ROC curve analysis, differences in neural vascular coupling dysfunction between AA and VDA were observed. These findings align with previously reported microstructural differences in two types of amblyopic visual pathways.[42,43] The occipital lobe region, compared to other brain regions, exhibits a greater presence of neural metabolic activity serving the visual pathway. Correlation analysis results indicate a negative association between the neurovascular coupling mechanism in the occipital lobe cortex of children with amblyopia and the BCVA of the contralateral eye, suggesting a close relationship between impaired neurovascular coupling function in amblyopia and functional disturbances in the visual cortex.

The activation of 5-HT1a receptors impedes long-term potentiation in the visual cortex, while the activation of 5-HT1b receptors is associated with changes in cortical responses induced by vision and the modulation of retinal synaptic function, leading to alterations in visual perception.[44–46] In the process of sensory circuit connections, SERT is involved in the regulation of activity-dependent mechanisms, refining

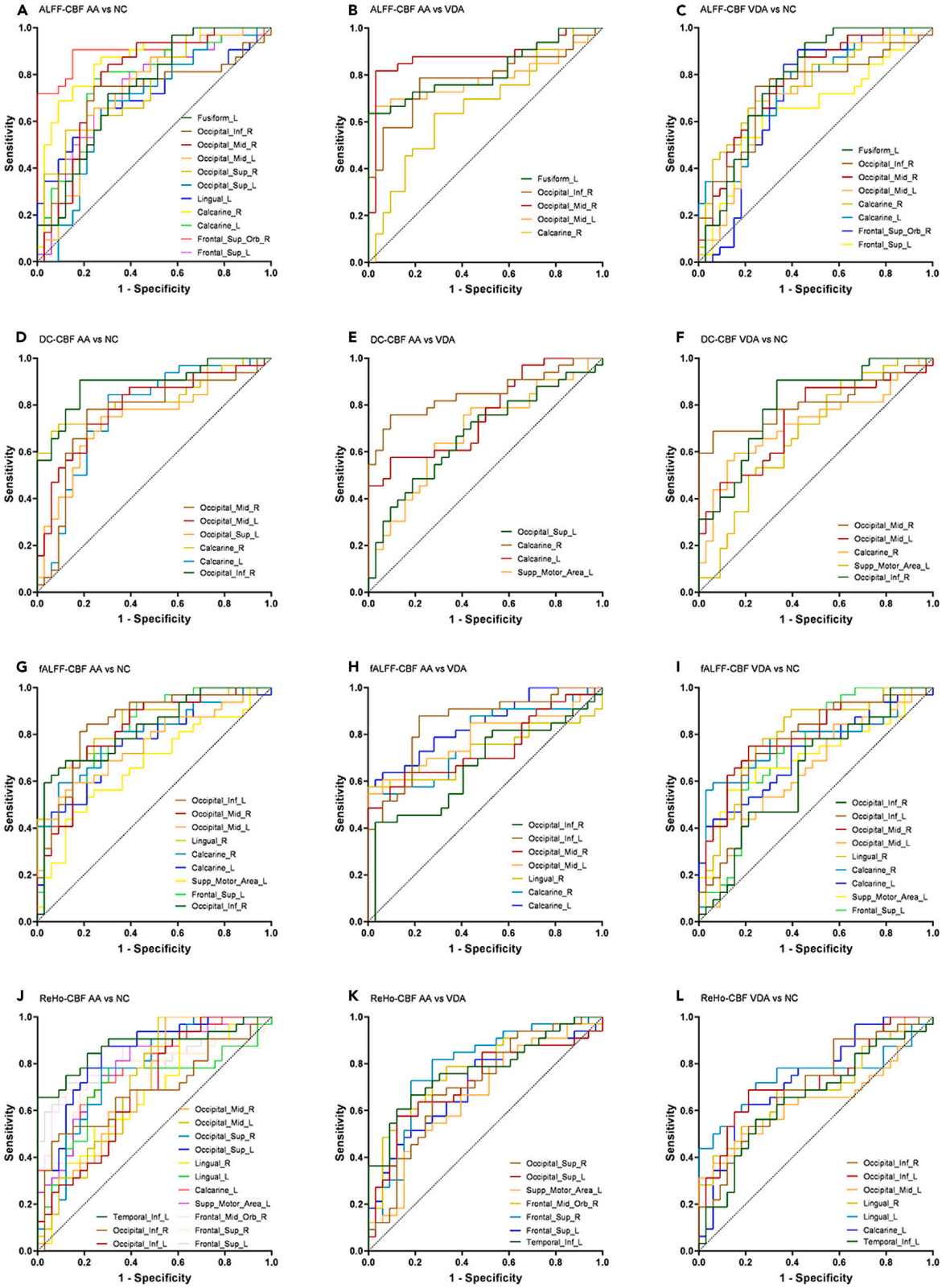
A ALFF-CBF AA vs NC
Fusiform_L
Occipital_Inf_R
Occipital_Mid_R
Occipital_Mid_L
Occipital_Sup_R
Occipital_Sup_L
Lingual_L
Calcarine_R
Calcarine_L
Frontal_Sup_Orb_R
Frontal_Sup_L
B ALFF-CBF AA vs VDA
Fusiform_L
Occipital_Inf_R
Occipital_Mid_R
Occipital_Mid_L
Calcarine_R
C ALFF-CBF VDA vs NC
Fusiform_L
Occipital_Inf_R
Occipital_Mid_R
Occipital_Mid_L
Calcarine_R
Calcarine_L
Frontal_Sup_Orb_R
Frontal_Sup_L
D DC-CBF AA vs NC
Occipital_Mid_R
Occipital_Mid_L
Occipital_Sup_L
Calcarine_R
Calcarine_L
Occipital_Inf_R
E DC-CBF AA vs VDA
Occipital_Sup_L
Calcarine_R
Calcarine_L
Supp_Motor_Area_L
F DC-CBF VDA vs NC
Occipital_Mid_R
Occipital_Mid_L
Calcarine_R
Supp_Motor_Area_L
Occipital_Inf_R
G fALFF-CBF AA vs NC
Occipital_Inf_L
Occipital_Mid_R
Occipital_Mid_L
Lingual_R
Calcarine_R
Calcarine_L
Supp_Motor_Area_L
Frontal_Sup_L
Occipital_Inf_R
H fALFF-CBF AA vs VDA
Occipital_Inf_R
Occipital_Inf_L
Occipital_Mid_R
Occipital_Mid_L
Lingual_R
Calcarine_R
Calcarine_L
I fALFF-CBF VDA vs NC
Occipital_Inf_R
Occipital_Inf_L
Occipital_Mid_R
Occipital_Mid_L
Lingual_R
Calcarine_R
Calcarine_L
Supp_Motor_Area_L
Frontal_Sup_L
J ReHo-CBF AA vs NC
Occipital_Mid_R
Occipital_Mid_L
Occipital_Sup_R
Occipital_Sup_L
Lingual_R
Lingual_L
Calcarine_L
Supp_Motor_Area_L
Temporal_Inf_L
Occipital_Inf_R
Occipital_Inf_L
Frontal_Mid_Orb_R
Frontal_Sup_R
Frontal_Sup_L
K ReHo-CBF AA vs VDA
Occipital_Sup_R
Occipital_Sup_L
Supp_Motor_Area_L
Frontal_Mid_Orb_R
Frontal_Sup_R
Frontal_Sup_L
Temporal_Inf_L
L ReHo-CBF VDA vs NC
Occipital_Inf_R
Occipital_Inf_L
Occipital_Mid_L
Lingual_R
Lingual_L
Calcarine_L
Temporal_Inf_L
Sensitivity
1 - Specificity

Figure 2. The performance of neurovascular coupling functional complex units corresponding to different brain regions on receiver operating characteristic curves between groups

(A–C) ALFF-CBF coupling in brain regions with significant distinctions in receiver operating characteristic curves between AA and NC groups (A), AA and VDA groups (B), VDA and NC groups (C). (D–F) DC-CBF coupling in brain regions with significant distinctions in receiver operating characteristic curves between AA and NC groups (D), AA and VDA groups (E), VDA and NC groups (F). (G–I) fALFF-CBF coupling in brain regions with significant distinctions in receiver operating characteristic curves between AA and NC groups (G), AA and VDA groups (H), VDA and NC groups (I). (J–L) ReHo-CBF coupling in brain regions with significant distinctions in receiver operating characteristic curves between AA and NC groups (J), AA and VDA groups (K), VDA and NC groups (L). For details of the brain region label, see Table S1.

Abbreviations: ALFF-CBF, amplitude of low-frequency fluctuation-cerebral blood flow; DC-CBF, degree centrality-cerebral blood flow; fALFF-CBF, fractional amplitude of low-frequency fluctuation-cerebral blood flow; ReHo-CBF, regional homogeneity-cerebral blood flow; AA, anisometropic amblyopia; VDA, visual deprivation amblyopia; NC, normal control.

the expression of specific inputs controlling visual targets.[47] The results of this study indicate that the effects of neurovascular coupling in both types of amblyopia are associated with dysregulation of the serotonergic circuitry. Although metabolism is not a characteristic of any disease, the aberrant uptake of CBF and the decoupling of the visual center are associated with abnormalities in the serotonin receptor system, indicating that the dysregulation of the amblyopic visual pathway is, to some extent, related to compensatory mechanisms of serotonin receptor metabolism dysfunction.[45,48] Dopamine, as a neurotransmitter, plays a crucial role in regulating visual development, lens contraction, and retinal adaptation.[49,50] It has been demonstrated that elevating dopamine levels or employing dopamine agonists has effects on refraction of the eye, consequently adjusting ocular refractive development.[51] Furthermore, the modulation of inhibitory circuits within the visual cortex has been found to be associated with the dopamine system, particularly involving D2 and DAT receptors.[52,53] Here, the neurovascular coupling impairments in two types of amblyopia have been demonstrated to be associated with dysfunction in the dopamine circuitry. Within the visual cortex, antagonists of the receptor mGluR5 block the long-term enhancement of excitatory synapses.[54] Of particular interest is the abnormal coupling of cortical neurons in the brain, which is associated with an increased release of metabotropic glutamate receptors, leading to an overabundance of impulsivity and functional impairments within the dopaminergic system pathway.[55] Each GABAa receptor consists of two α subunits and three other subunits. Different α subunits contribute distinct functions during the developmental process of the mouse visual cortex, generating heterogeneity among the α subunits during accelerated neocortical development, thereby enhancing γ-aminobutyric acid-mediated transmission and resulting in reactive loss of visual acuity.[56,57] The NAT regulates visual transmission activity, influencing the executive functions of the visual cortex.[58] Indeed, the findings of this study

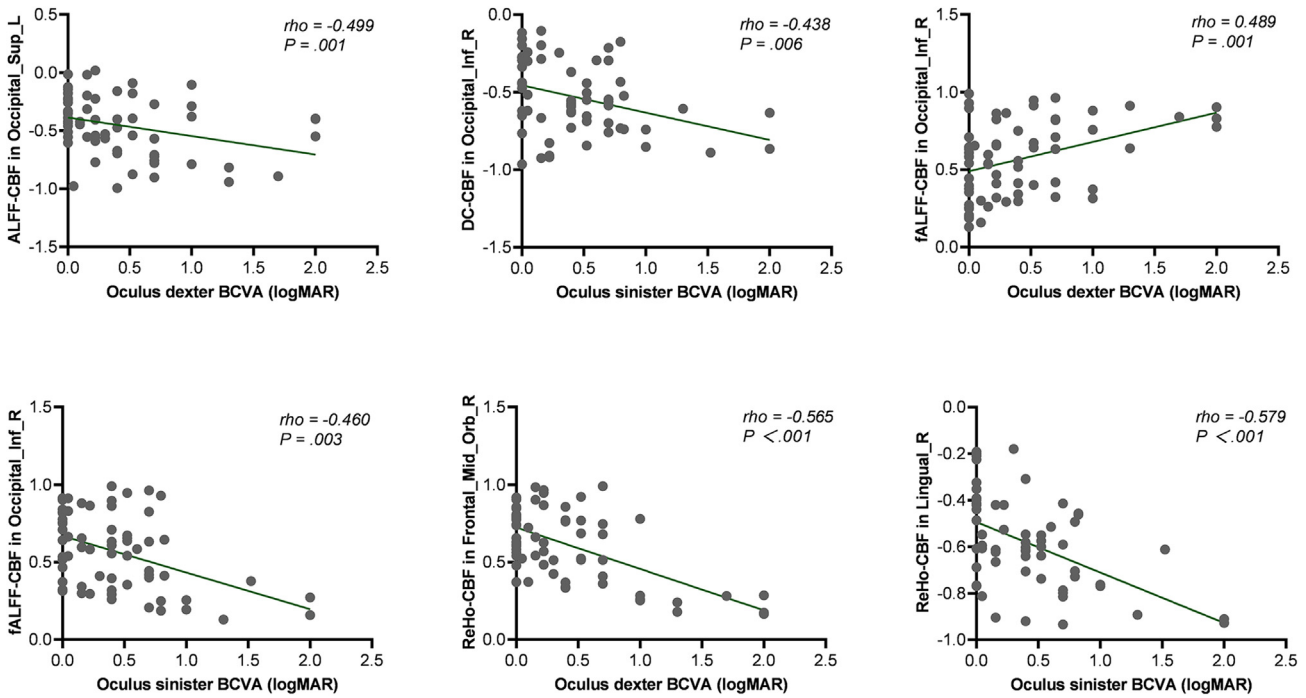

Figure 3. Spearman correlation analysis of neurovascular coupling changes in brain regions and BCVA

For details of the brain region label, see Table S1.

Abbreviations: ALFF-CBF, amplitude of low-frequency fluctuation-cerebral blood flow; DC-CBF, degree centrality-cerebral blood flow; fALFF-CBF, fractional amplitude of low-frequency fluctuation-cerebral blood flow; ReHo-CBF, regional homogeneity-cerebral blood flow; BCVA, best-corrected visual acuity.

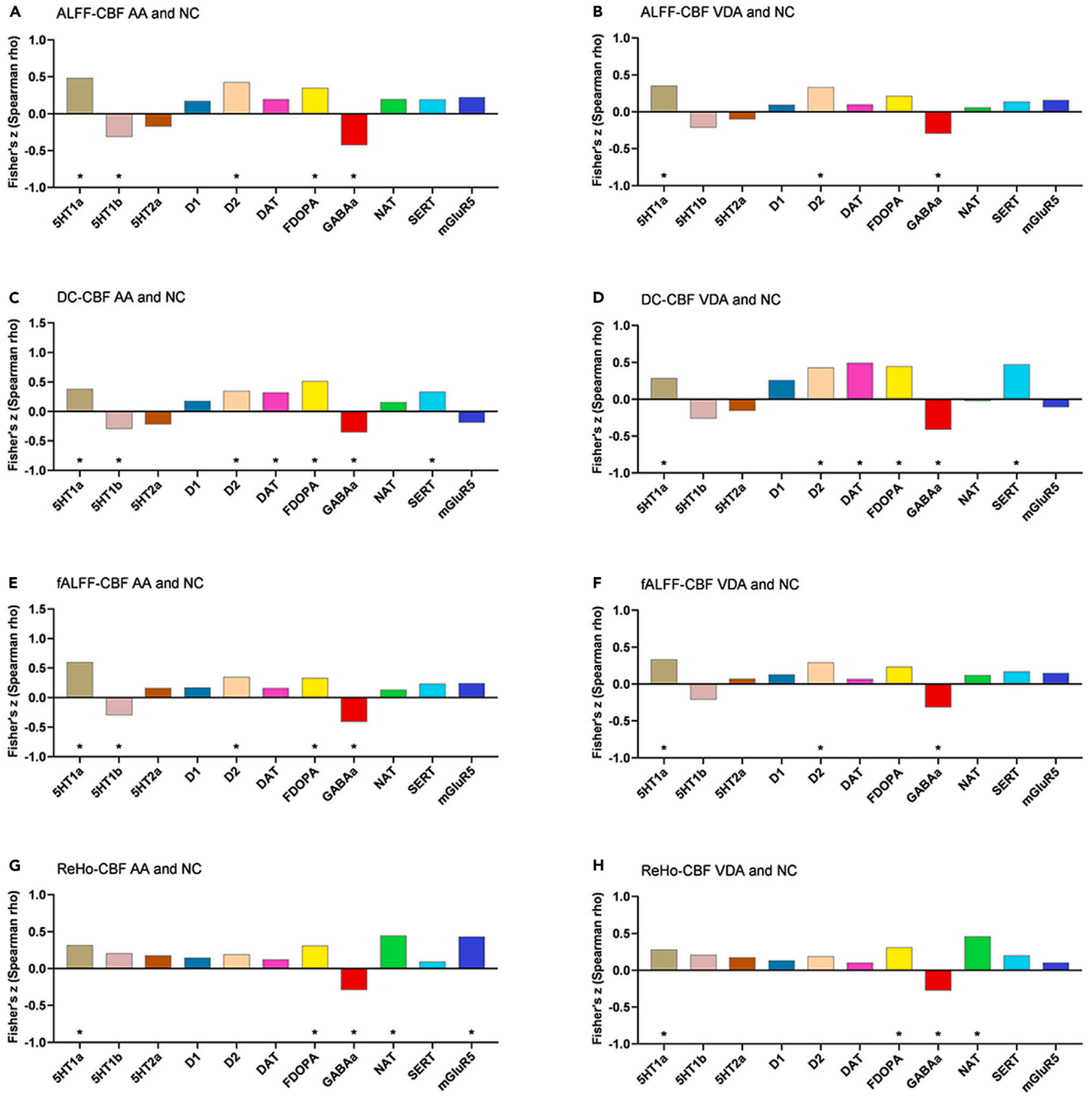

Figure 4. The association between neurovascular coupling effect with receptor/transporter densities

(A and B) Correlations between effect sizes of ALFF-CBF coupling and receptor systems, for AA and NC groups (A), VDA and NC groups (B). (C and D) Correlations between effect sizes of DC-CBF coupling and receptor systems, for AA and NC groups (C), VDA and NC groups (D). (E and F) Correlations between effect sizes of fALFF-CBF coupling and receptor systems, for AA and NC groups (E), VDA and NC groups (F). (G and H) Correlations between effect sizes of ReHo-CBF coupling and receptor systems, for AA and NC groups (G), VDA and NC groups (H). The "*" represented that the correlation was significant ($p < 0.05$ for permutation, $N = 10{,}000$ permutations).

Abbreviations: ALFF-CBF, amplitude of low-frequency fluctuation-cerebral blood flow; DC-CBF, degree centrality-cerebral blood flow; fALFF-CBF, fractional amplitude of low-frequency fluctuation-cerebral blood flow; ReHo-CBF, regional homogeneity-cerebral blood flow; AA, anisometropic amblyopia; VDA, visual deprivation amblyopia; NC, normal control.

indicate an association between two kinds of amblyopia neurovascular coupling effects and vulnerability in NAT and GABAa neurotransmitter systems.

In summary, the evidence of alterations in neurovascular coupling in children with AA and VDA is revealed by the results of this study, and the association with the neurotransmitter information is assessed. These findings provide new multimodal neuroimaging evidence for unique associations between nerves, blood flow, neurotransmitters, and executive functions in two types of amblyopic individuals. Describing the neurovascular coupling mechanisms in children with amblyopia may contribute to the development of personalized neural therapies.

Limitations of the study

The neurovascular coupling mechanisms and potential molecular basis of AA and VDA were reported from multiple perspectives in this study. However, there are still some limitations in this research. Firstly, a cross-sectional design was employed without deliberate inclusion of the severity of amblyopia in the relevant variables. It is noteworthy that the primary objective of this study did not involve assessing the relationship between the severity of amblyopia and neurovascular coupling mechanisms. Secondly, previous authors have interpreted ALFF-CBF, DC-CBF, fALFF-CBF, and ReHo-CBF coupling as representatives of neurovascular coupling, but we were unable to directly measure neurovascular coupling.[22–24] While positron emission tomography (PET) is commonly considered the gold standard for measuring blood flow, the practice of relying on alternative measurements to describe the neurovascular coupling in the body is deemed reasonable, given the potential radiation risks of PET scans in children.[24] Thirdly, although ASL and BOLD signals are acquired during the same scanning process, there still exists a certain time lag. However, since neither neural function measurement nor CBF mapping is influenced by time, the impact of this limitation on our results can be considered negligible. Lastly, while research findings indicate a correlation between the magnitude of neurovascular coupling effects and receptor/transporter density, it is noteworthy that the information provided by JuSpace, serving as a framework linking neural imaging data and potential neurotransmitter information, has certain limitations.[59] Future studies should integrate with clinical trials to offer more direct evidence.

STAR★METHODS

Detailed methods are provided in the online version of this paper and include the following:

- KEY RESOURCES TABLE
- RESOURCE AVAILABILITY
  - Lead contact
  - Materials availability
  - Data and code availability
- EXPERIMENTAL MODEL AND STUDY PARTICIPANT DETAILS
  - Ethics statement
  - Inclusion criteria and exclusion criteria
- METHOD DETAILS
  - Ophthalmic examination method details
  - MRI data acquisition method details
  - Imaging analysis
  - Neurovascular coupling analysis
- QUANTIFICATION AND STATISTICAL ANALYSIS

SUPPLEMENTAL INFORMATION

Supplemental information can be found online at https://doi.org/10.1016/j.isci.2024.109988.

ACKNOWLEDGMENTS

This study was supported by Grant 232102310094 from Henan Provincial Science and Technology Research Project, Grant LHGJ20230217 from Medical science and technology research project of Henan province, Grant U23A20437 from the National Natural Science Foundation of China, and Grant YNQN2017160 from The First Affiliated Hospital of Zhengzhou University.

AUTHOR CONTRIBUTIONS

Concept and design, X.Z., L.L., S.H., and B.W.; acquisition, analysis, or interpretation of the data, all authors; drafting of the manuscript, X.Z.; critical revision of the manuscript for important intellectual content, all authors; statistical analysis, X.Z. and L.L.; administrative, technical, or material support, M.W., Y.Z., J.C., and B.W.; supervision, G.Z. and J.C.

DECLARATION OF INTERESTS

The authors declare no competing interests.

Received: February 7, 2024
Revised: April 14, 2024
Accepted: May 13, 2024
Published: May 16, 2024

REFERENCES

1. Choi, M.Y., Lee, K.M., Hwang, J.M., Choi, D.G., Lee, D.S., Park, K.H., and Yu, Y.S. (2001). Comparison between anisometropic and strabismic amblyopia using functional magnetic resonance imaging. Br. J. Ophthalmol. *85*, 1052–1056. https://doi.org/10.1136/bjo.85.9.1052.
2. Bennett, C.R., Bauer, C.M., Bailin, E.S., and Merabet, L.B. (2020). Neuroplasticity in cerebral visual impairment (CVI): Assessing functional vision and the neurophysiological correlates of dorsal stream dysfunction. Neurosci. Biobehav. Rev. *108*, 171–181. https://doi.org/10.1016/j.neubiorev.2019.10.011.
3. Demer, J.L., von Noorden, G.K., Volkow, N.D., and Gould, K.L. (1988). Imaging of Cerebral Blood Flow and Metabolism in Amblyopia by Positron Emission Tomography. Am. J. Ophthalmol. *105*, 337–347. https://doi.org/10.1016/0002-9394(88)90294-2.
4. Hoyt, C.S. (2005). Amblyopia: A Neuro-Ophthalmic View. J. Neuro Ophthalmol. *25*, 227–231. https://doi.org/10.1097/01.wno.0000177304.67715.ba.
5. Li, C., Cheng, L., Yu, Q., Xie, B., and Wang, J. (2012). Relationship of Visual Cortex Function and Visual Acuity in Anisometropic Amblyopic Children. Int. J. Med. Sci. *9*, 115–120. https://doi.org/10.7150/ijms.9.115.
6. Pescosolido, N., Stefanucci, A., Buomprisco, G., and Fazio, S. (2014). Amblyopia treatment strategies and new drug therapies. J. Pediatr. Ophthalmol. Strabismus *51*, 78–86. https://doi.org/10.3928/01913913-20130107-01.
7. Huh, C.Y.L., Abdelaal, K., Salinas, K.J., Gu, D., Zeitoun, J., Figueroa Velez, D.X., Peach, J.P., Fowlkes, C.C., and Gandhi, S.P. (2020). Long-term Monocular Deprivation during Juvenile Critical Period Disrupts Binocular Integration in Mouse Visual Thalamus. J. Neurosci. *40*, 585–604. https://doi.org/10.1523/JNEUROSCI.1626-19.2019.
8. Zhai, J., Chen, M., Liu, L., Zhao, X., Zhang, H., Luo, X., and Gao, J. (2013). Perceptual learning treatment in patients with anisometropic amblyopia: a neuroimaging study. Br. J. Ophthalmol. *97*, 1420–1424. https://doi.org/10.1136/bjophthalmol-2013-303778.
9. Prusky, G.T., and Douglas, R.M. (2003). Developmental plasticity of mouse visual acuity. Eur. J. Neurosci. *17*, 167–173. https://doi.org/10.1046/j.1460-9568.2003.02420.x.
10. Hensch, T.K. (2005). Critical period plasticity in local cortical circuits. Nat. Rev. Neurosci. *6*, 877–888. https://doi.org/10.1038/nrn1787.
11. Khibnik, L.A., Cho, K.K.A., and Bear, M.F. (2010). Relative Contribution of Feedforward Excitatory Connections to Expression of Ocular Dominance Plasticity in Layer 4 of Visual Cortex. Neuron *66*, 493–500. https://doi.org/10.1016/j.neuron.2010.04.012.
12. Duffy, K.R., Bear, M.F., Patel, N.B., Das, V.E., and Tychsen, L. (2023). Human deprivation amblyopia: treatment insights from animal models. Front. Neurosci. *17*, 1249466. https://doi.org/10.3389/fnins.2023.1249466.
13. Sabel, B.A., Flammer, J., and Merabet, L.B. (2018). Residual vision activation and the brain-eye-vascular triad: Dysregulation, plasticity and restoration in low vision and blindness - a review. Restor. Neurol. Neurosci. *36*, 767–791. https://doi.org/10.3233/RNN-180880.
14. Kaplan, L., Chow, B.W., and Gu, C. (2020). Neuronal regulation of the blood–brain barrier and neurovascular coupling. Nat. Rev. Neurosci. *21*, 416–432. https://doi.org/10.1038/s41583-020-0322-2.
15. Attwell, D., Buchan, A.M., Charpak, S., Lauritzen, M., MacVicar, B.A., and Newman, E.A. (2010). Glial and neuronal control of brain blood flow. Nature *468*, 232–243. https://doi.org/10.1038/nature09613.
16. Hernandez-Garcia, L., Lahiri, A., and Schollenberger, J. (2019). Recent progress in ASL. Neuroimage *187*, 3–16. https://doi.org/10.1016/j.neuroimage.2017.12.095.
17. Haller, S., Zaharchuk, G., Thomas, D.L., Lovblad, K.O., Barkhof, F., and Golay, X. (2016). Arterial Spin Labeling Perfusion of the Brain: Emerging Clinical Applications. Radiology *281*, 337–356. https://doi.org/10.1148/radiol.2016150789.
18. Baek, E.C., Hyon, R., López, K., Finn, E.S., Porter, M.A., and Parkinson, C. (2022). In-degree centrality in a social network is linked to coordinated neural activity. Nat. Commun. *13*, 1118. https://doi.org/10.1038/s41467-022-28432-3.
19. Zang, Y., Jiang, T., Lu, Y., He, Y., and Tian, L. (2004). Regional homogeneity approach to fMRI data analysis. Neuroimage *22*, 394–400. https://doi.org/10.1016/j.neuroimage.2003.12.030.
20. Baria, A.T., Baliki, M.N., Parrish, T., and Apkarian, A.V. (2011). Anatomical and Functional Assemblies of Brain BOLD Oscillations. J. Neurosci. *31*, 7910–7919. https://doi.org/10.1523/JNEUROSCI.1296-11.2011.
21. Zou, Q.H., Zhu, C.Z., Yang, Y., Zuo, X.N., Long, X.Y., Cao, Q.J., Wang, Y.F., and Zang, Y.F. (2008). An improved approach to detection of amplitude of low-frequency fluctuation (ALFF) for resting-state fMRI: Fractional ALFF. J. Neurosci. Methods *172*, 137–141. https://doi.org/10.1016/j.jneumeth.2008.04.012.
22. Li, P., Ma, S., Ma, X., Ding, D., Zhu, X., Zhang, H., Liu, J., Mu, J., and Zhang, M. (2023). Reversal of neurovascular decoupling and cognitive impairment in patients with end-stage renal disease during a hemodialysis session: Evidence from a comprehensive fMRI analysis. Hum. Brain Mapp. *44*, 989–1001. https://doi.org/10.1002/hbm.26122.
23. Zhang, X., Liu, L., Yang, F., Liu, Z., Jin, X., Han, S., Zhang, Y., Cheng, J., and Wen, B. (2024). Neurovascular coupling dysfunction in high myopia patients: Evidence from a multi-modal magnetic resonance imaging analysis. J. Neuroradiol. *51*, 281–289. https://doi.org/10.1016/j.neurad.2023.09.005.
24. Baller, E.B., Valcarcel, A.M., Adebimpe, A., Alexander-Bloch, A., Cui, Z., Gur, R.C., Gur, R.E., Larsen, B.L., Linn, K.A., O'Donnell, C.M., et al. (2022). Developmental coupling of cerebral blood flow and fMRI fluctuations in youth. Cell Rep. *38*, 110576. https://doi.org/10.1016/j.celrep.2022.110576.
25. Birch, E.E., Castañeda, Y.S., Cheng-Patel, C.S., Morale, S.E., Kelly, K.R., and Wang, S.X. (2020). Self-perception in Preschool Children With Deprivation Amblyopia and Its Association With Deficits in Vision and Fine Motor Skills. JAMA Ophthalmol. *138*, 1307–1310. https://doi.org/10.1001/jamaophthalmol.2020.4363.
26. Qi, S., Mu, Y.F., Cui, L.B., Li, R., Shi, M., Liu, Y., Xu, J.Q., Zhang, J., Yang, J., and Yin, H. (2016). Association of Optic Radiation Integrity with Cortical Thickness in Children with Anisometropic Amblyopia. Neurosci. Bull. *32*, 51–60. https://doi.org/10.1007/s12264-015-0005-6.
27. Hasel, P., Dando, O., Jiwaji, Z., Baxter, P., Todd, A.C., Heron, S., Márkus, N.M., McQueen, J., Hampton, D.W., Torvell, M., et al. (2017). Neurons and neuronal activity control gene expression in astrocytes to regulate their development and metabolism. Nat. Commun. *8*, 15132. https://doi.org/10.1038/ncomms15132.
28. Abbott, N.J., Patabendige, A.A.K., Dolman, D.E.M., Yusof, S.R., and Begley, D.J. (2010). Structure and function of the blood–brain barrier. Neurobiol. Dis. *37*, 13–25. https://doi.org/10.1016/j.nbd.2009.07.030.
29. Fields, R.D., and Stevens-Graham, B. (2002). New Insights into Neuron-Glia Communication. Science *298*, 556–562. https://doi.org/10.1126/science.298.5593.556.
30. Li, M., Newton, A.T., Anderson, A.W., Ding, Z., and Gore, J.C. (2019). Characterization of the hemodynamic response function in white matter tracts for event-related fMRI. Nat. Commun. *10*, 1140. https://doi.org/10.1038/s41467-019-09076-2.
31. Sabayan, B., and Westendorp, R.G.J. (2021). Neurovascular-glymphatic dysfunction and white matter lesions. GeroScience *43*, 1635–1642. https://doi.org/10.1007/s11357-021-00361-x.
32. Tomassy, G.S., Berger, D.R., Chen, H.H., Kasthuri, N., Hayworth, K.J., Vercelli, A., Seung, H.S., Lichtman, J.W., and Arlotta, P. (2014). Distinct Profiles of Myelin Distribution Along Single Axons of Pyramidal Neurons in the Neocortex. Science *344*, 319–324. https://doi.org/10.1126/science.1249766.
33. Mathias, E.J., Kenny, A., Plank, M.J., and David, T. (2018). Integrated models of neurovascular coupling and BOLD signals: Responses for varying neural activations. Neuroimage *174*, 69–86. https://doi.org/10.1016/j.neuroimage.2018.03.010.
34. Rossi, D.J. (2006). Another BOLD role for astrocytes: coupling blood flow to neural activity. Nat. Neurosci. *9*, 159–161. https://doi.org/10.1038/nn0206-159.
35. Zuo, X.N., Di Martino, A., Kelly, C., Shehzad, Z.E., Gee, D.G., Klein, D.F., Castellanos, F.X., Biswal, B.B., and Milham, M.P. (2010). The

oscillating brain: Complex and reliable. Neuroimage *49*, 1432–1445. https://doi.org/10.1016/j.neuroimage.2009.09.037.

36. Zuo, X.N., Ehmke, R., Mennes, M., Imperati, D., Castellanos, F.X., Sporns, O., and Milham, M.P. (2012). Network Centrality in the Human Functional Connectome. Cereb. Cortex *22*, 1862–1875. https://doi.org/10.1093/cercor/bhr269.
37. Zuo, X.N., Xu, T., Jiang, L., Yang, Z., Cao, X.Y., He, Y., Zang, Y.F., Castellanos, F.X., and Milham, M.P. (2013). Toward reliable characterization of functional homogeneity in the human brain: Preprocessing, scan duration, imaging resolution and computational space. Neuroimage *65*, 374–386. https://doi.org/10.1016/j.neuroimage.2012.10.017.
38. Li, P., Mu, J., Ma, X., Ding, D., Ma, S., Zhang, H., Liu, J., and Zhang, M. (2021). Neurovascular coupling dysfunction in end-stage renal disease patients related to cognitive impairment. J. Cereb. Blood Flow Metab. *41*, 2593–2606. https://doi.org/10.1177/0271678X211007960.
39. Iadecola, C., and Nedergaard, M. (2007). Glial regulation of the cerebral microvasculature. Nat. Neurosci. *10*, 1369–1376. https://doi.org/10.1038/nn2003.
40. Shokri-Kojori, E., Tomasi, D., Alipanahi, B., Wiers, C.E., Wang, G.J., and Volkow, N.D. (2019). Correspondence between cerebral glucose metabolism and BOLD reveals relative power and cost in human brain. Nat. Commun. *10*, 690. https://doi.org/10.1038/s41467-019-08546-x.
41. Archila-Meléndez, M.E., Sorg, C., and Preibisch, C. (2020). Modeling the impact of neurovascular coupling impairments on BOLD-based functional connectivity at rest. Neuroimage *218*, 116871. https://doi.org/10.1016/j.neuroimage.2020.116871.
42. Mitchell, D.E., and Sengpiel, F. (2009). Neural mechanisms of recovery following early visual deprivation. Philos. Trans. R. Soc. Lond. B Biol. Sci. *364*, 383–398. https://doi.org/10.1098/rstb.2008.0192.
43. Pons, C., Jin, J., Mazade, R., Dul, M., Zaidi, Q., and Alonso, J.M. (2019). Amblyopia Affects the ON Visual Pathway More than the OFF. J. Neurosci. *39*, 6276–6290. https://doi.org/10.1523/JNEUROSCI.3215-18.2019.
44. Pickard, G.E., Smith, B.N., Belenky, M., Rea, M.A., Dudek, F.E., and Sollars, P.J. (1999). 5-HT_{1B} receptor-mediated presynaptic inhibition of retinal input to the suprachiasmatic nucleus. J. Neurosci. *19*, 4034–4045. https://doi.org/10.1523/JNEUROSCI.19-10-04034.1999.
45. Shimegi, S., Kimura, A., Sato, A., Aoyama, C., Mizuyama, R., Tsunoda, K., Ueda, F., Araki, S., Goya, R., and Sato, H. (2016). Cholinergic and serotonergic modulation of visual information processing in monkey V1. J. Physiol. Paris *110*, 44–51. https://doi.org/10.1016/j.jphysparis.2016.09.001.
46. Edagawa, Y., Saito, H., and Abe, K. (1998). 5-HT1A receptor-mediated inhibition of long-term potentiation in rat visual cortex. Eur. J. Pharmacol. *349*, 221–224. https://doi.org/10.1016/S0014-2999(98)00286-6.
47. García-Frigola, C., and Herrera, E. (2010). Zic2 regulates the expression of Sert to modulate eye-specific refinement at the visual targets. EMBO J. *29*, 3170–3183. https://doi.org/10.1038/emboj.2010.172.
48. Zhou, W., and Sabel, B.A. (2023). Vascular dysregulation in glaucoma: retinal vasoconstriction and normal neurovascular coupling in altitudinal visual field defects. EPMA J. *14*, 87–99. https://doi.org/10.1007/s13167-023-00316-6.
49. Dearry, A., Edelman, J.L., Miller, S., and Burnside, B. (1990). Dopamine induces light-adaptive retinomotor movements in bullfrog cones via D2 receptors and in retinal pigment epithelium via D1 receptors. J. Neurochem. *54*, 1367–1378. https://doi.org/10.1111/j.1471-4159.1990.tb01971.x.
50. Zhou, X., Pardue, M.T., Iuvone, P.M., and Qu, J. (2017). Dopamine signaling and myopia development: What are the key challenges. Prog. Retin. Eye Res. *61*, 60–71. https://doi.org/10.1016/j.preteyeres.2017.06.003.
51. Shu, Z., Chen, K., Wang, Q., Wu, H., Zhu, Y., Tian, R., Yan, W., Huang, Q., Zhang, C., Xiong, W., et al. (2023). The Role of Retinal Dopamine D1 Receptors in Ocular Growth and Myopia Development in Mice. J. Neurosci. *43*, 8231–8242. https://doi.org/10.1523/JNEUROSCI.1196-23.2023.
52. Davis, M.F., Figueroa Velez, D.X., Guevarra, R.P., Yang, M.C., Habeeb, M., Carathedathu, M.C., and Gandhi, S.P. (2015). Inhibitory Neuron Transplantation into Adult Visual Cortex Creates a New Critical Period that Rescues Impaired Vision. Neuron *86*, 1055–1066. https://doi.org/10.1016/j.neuron.2015.03.062.
53. Montardy, Q., Zhou, Z., Li, L., Yang, Q., Lei, Z., Feng, X., Chen, S., Shi, Q., Zhang, H., Chen, S., et al. (2022). Dopamine modulates visual threat processing in the superior colliculus via D2 receptors. iScience *25*, 104388. https://doi.org/10.1016/j.isci.2022.104388.
54. Sarihi, A., Jiang, B., Komaki, A., Sohya, K., Yanagawa, Y., and Tsumoto, T. (2008). Metabotropic Glutamate Receptor Type 5-Dependent Long-Term Potentiation of Excitatory Synapses on Fast-Spiking GABAergic Neurons in Mouse Visual Cortex. J. Neurosci. *28*, 1224–1235. https://doi.org/10.1523/JNEUROSCI.4928-07.2008.
55. Selemon, L.D. (2013). A role for synaptic plasticity in the adolescent development of executive function. Transl. Psychiatry *3*, e238. https://doi.org/10.1038/tp.2013.7.
56. Fagiolini, M., Fritschy, J.M., Löw, K., Möhler, H., Rudolph, U., and Hensch, T.K. (2004). Specific GABAA Circuits for Visual Cortical Plasticity. Science *303*, 1681–1683. https://doi.org/10.1126/science.1091032.
57. Bosman, L.W.J., Rosahl, T.W., and Brussaard, A.B. (2002). Neonatal development of the rat visual cortex: synaptic function of GABAa receptor α subunits. J. Physiol. *545*, 169–181. https://doi.org/10.1113/jphysiol.2002.026534.
58. Gelbard-Sagiv, H., Magidov, E., Sharon, H., Hendler, T., and Nir, Y. (2018). Noradrenaline Modulates Visual Perception and Late Visually Evoked Activity. Curr. Biol. *28*, 2239–2249.e6. https://doi.org/10.1016/j.cub.2018.05.051.
59. Dukart, J., Holiga, S., Rullmann, M., Lanzenberger, R., Hawkins, P.C.T., Mehta, M.A., Hesse, S., Barthel, H., Sabri, O., Jech, R., and Eickhoff, S.B. (2021). JuSpace: A tool for spatial correlation analyses of magnetic resonance imaging data with nuclear imaging derived neurotransmitter maps. Hum. Brain Mapp. *42*, 555–566. https://doi.org/10.1002/hbm.25244.
60. Yan, C.G., Wang, X.D., Zuo, X.N., and Zang, Y.F. (2016). DPABI: Data Processing & Analysis for (Resting-State) Brain Imaging. Neuroinformatics *14*, 339–351. https://doi.org/10.1007/s12021-016-9299-4.
61. Mutsaerts, H.J.M.M., Petr, J., Groot, P., Vandemaele, P., Ingala, S., Robertson, A.D., Václavů, L., Groote, I., Kuijf, H., Zelaya, F., et al. (2020). ExploreASL: An image processing pipeline for multi-center ASL perfusion MRI studies. Neuroimage *219*, 117031. https://doi.org/10.1016/j.neuroimage.2020.117031.

STAR★METHODS

KEY RESOURCES TABLE

REAGENT or RESOURCE	SOURCE	IDENTIFIER
Deposited data		
receptors/transporters data	Dukart et al.[59]	https://github.com/juryxy/JuSpace
Software and algorithms		
Data Processing Assistant for Resting-State fMRI (DPARSF) V4.3	https://rfmri.org/	https://rfmri.org/DPARSF
Statistical Product and Service Solutions (SPSS 23.0)	The IBM SPSS software platform	https://www.ibm.com/spss
ExploreASL V1.10.1	http://www.exploreasl.org/	https://github.com/ExploreASL/ExploreASL
JuSpace V1.4	https://github.com/	https://github.com/juryxy/JuSpace

RESOURCE AVAILABILITY

Lead contact

Further information and requests for resources and reagents should be directed to and will be fulfilled by the lead contact, Baohong Wen (fccwenbh@zzu.edu.cn).

Materials availability

This study did not generate new unique reagents.

Data and code availability

- The receptors/transporters data is publicly available. The DOI is listed in the key resources table.
- This paper does not report original code.
- Any additional information required to reanalyze the data reported in this paper is available from the lead contact upon request.

EXPERIMENTAL MODEL AND STUDY PARTICIPANT DETAILS

Ethics statement

This study followed the tenets of the Declaration of Helsinki, and was approved by the First Affiliated Hospital of Zhengzhou University Scientific research and clinical trial ethics committee (No: 2022-KY-0394-002).

A total of 97 participants (AA = 32 [sixteen males and sixteen females], VDA = 33 [sixteen males and seventeen females], NC = 32 [sixteen males and sixteen females]) from the Chinese population were included. The inclusion criteria and exclusion criteria were as follows.

Inclusion criteria and exclusion criteria

AA and VDA group

Inclusion criteria encompassed individuals who met the following prerequisites: a confirmed diagnosis of AA, that is, binocular hyperopic refractive error, the spherical power diopter difference between the two eyes was ≥1.50 D, or the cylindrical power diopter difference was ≥1.00 D. Confirmed diagnosis of VDA, that is, unilateral or bilateral amblyopia is caused by form deprivation factors such as refractive interstitial opacity, congenital ptosis, and inappropriate masking. The age ranged from 5 to 16 years, not previously been treated for amblyopia, and be able to complete examinations conducted for this study under natural conditions (without sedation and hypnosis). Exclusion criteria consisted of patients with underlying neurological or psychiatric conditions, a history of ocular or cranial surgical interventions, and those incapable of complying with the experimental procedures.

NC group

The visual acuity of both eyes was ≥ 0.8, age ranged from 5 to 16 years. The ability to actively participate in the examinations conducted for this study. Exclusion criteria consisted of patients with underlying neurological or psychiatric conditions, a history of ocular or cranial surgical interventions, and those incapable of complying with the experimental procedures.

METHOD DETAILS

Ophthalmic examination method details

The assessment of BCVA at a distance of 5 meters was performed using the international standard logarithmic visual acuity chart. The intraocular pressure was assessed using the CT-80A non-contact tonometer (TOPCON, Japan). Participants were administered Tropicamide Phenylephrine eye drops (Shenyang Xingqi Pharmaceutical Co., LTD., China) at ten-minute intervals for a total of four administrations. Optometry was performed with RM-8000 refractometer (TOPCON, Japan). The visual acuity and BCVA were transformed into logarithm of the minimum angle of resolution (logMAR) for quantitative analysis. Refractive error was described by diopter of spherical power and diopter of cylindrical power.

MRI data acquisition method details

Images were acquired using a Siemens Prisma 3.0T superconductor magnetic resonance imaging system equipped with a 64-channel magnetic head-and-neck coil. Participants were positioned in a supine orientation with their heads inward and instructed to maintain wakefulness while keeping their eyes closed. BOLD functional magnetic resonance imaging (fMRI) data were obtained through a gradient-echo planar imaging approach, with the following parameters: echo time = 30.0 ms, repetition time = 1000 ms, matrix size = 110 × 110, slice thickness = 2.2 mm, flip angle = 70°, 52 contiguous slices, and a total of 400 time points. The total acquisition time for this fMRI scan was 6 minutes and 52 seconds. ASL sequence was performed using a 3-dimensional fast spin-echo acquisition, with the following parameters: echo time = 16.18 ms, repetition time = 4600 ms, field of view = 192 × 192 mm^2, slice thickness = 3.0 mm, flip angle = 180°, and 40 contiguous slices. The total acquisition time for this ASL scan was 4 minutes and 59 seconds. Furthermore, T1-weighted images of the entire brain were procured utilizing a 3-dimensional high-resolution sagittal sequence, employing the following settings: echo time = 2.32 ms, repetition time = 2300 ms, matrix size = 256 × 256, slice thickness = 0.9 mm, flip angle = 8°, and 176 contiguous slices. The complete acquisition duration for the T1-weighted image acquisition was 5 minutes and 21 seconds.

Imaging analysis

The Data Processing Assistant for Resting-State fMRI (DPARSF) toolbox, executed on the MATLAB R2019a platform from MathWorks, based in the USA, was employed for the preprocessing of fMRI images.[60] The DC, ReHo, ALFF, and fALFF were computed using standard procedures based on neural indices. The corresponding CBF maps were obtained by processing ASL images using ExploreASL.[61] Non-brain tissues were excluded and the CBF was normalized. Details of the imaging analysis procedures were as follows.

BOLD Image Preprocessing Procedure

To eliminate the effects of initial scanning instability factors, the initial 10 time points' images were excluded; Head motion correction was carried out, and subjects exceeding a 2° rotation or a 2 mm shift were excluded. Normalized images to a standard Montreal Neurological Institute spatial template and resampled voxels to 3 × 3 × 3 mm^3; Spatial smoothing utilized a Gaussian kernel of 6 mm full-width at half-maximum. To eliminate the linear drift stemming from thermal noise in the imager, a correction was applied. Further, the signals from white matter and cerebrospinal fluid were separately averaged, and interference covariates were regressed.

Neural Index Calculation Procedure

ALFF and fALFF maps were calculated without the procedure of band-pass filtering. The time series was first converted into the frequency domain power spectrum using a fast Fourier transform. The square root of the power spectrum was calculated, and each voxel within the range of 0.01-0.08 Hz was averaged. The average square root of the power spectrum was ALFF. The average ALFF value of the whole brain voxel level was subtracted from the voxel-level ALFF map of the subject, and then divided by the standard deviation. On this basis, the ratio of the root mean square of the power spectrum in the low-frequency range (0.01-0.08 Hz) of ALFF to the root mean square of the power spectrum of the whole frequency was used to obtain the fALFF. After such a Z transformation, the standardized ALFF and fALFF maps were obtained.[35] Spatial smoothing was not performed to avoid artificial local connections in DC map. The functional network at the voxel level was constructed, taking each voxel as a node and calculating its correlation with other nodes in the whole brain. A threshold of 0.25 was set to exclude voxels with weak correlations. Counting the number of significant suprathreshold (0.25) correlations (number of edges) for each subject resulted in a DC value with a weight property. The obtained DC values were normalized by subtracting the whole brain mean and dividing by the whole brain standard deviation, resulting in a standardized DC map of z-score mapping.[36] For voxels, the response at each time point was transformed into a rank sequence. The statistical value of this rank sequence was the ReHo value, which was a non-parametric value. The obtained ReHo value was normalized by subtracting the average value of the whole brain and then dividing by the standard deviation of the whole brain, to obtain the standardized ReHo map.[37]

CBF Calculation Procedure

The CBF brain images were co-registered to the corresponding T1 structural images. The CBF images were spatially normalized to the standard MNI space and resampled to a 3 × 3 × 3 mm^3 resolution. Spatial smoothing was performed using a Gaussian kernel of 6 mm full-width at half-maximum. The resulting images were transformed using a Z transformation approach.

Neurovascular coupling analysis

The brain was divided into 90 regions using the recognized and reliable Automated Anatomical Labeling atlas. The spatial correlation coefficients between neuronal activity and cerebral perfusion in each brain region were calculated. Four types of neurovascular coupling functional complex units (DC-CBF, ReHo-CBF, ALFF-CBF and fALFF-CBF) are constructed.

QUANTIFICATION AND STATISTICAL ANALYSIS

Clinical indicators and demographic data underwent an assessment for normal distribution. For normally distributed continuous variables, descriptive statistics included mean values along with their corresponding standard deviations. Group comparisons were conducted utilizing a one-way analysis of variance (ANOVA). Non-normally distributed variables were presented as medians accompanied by interquartile ranges, and group comparisons were executed using the Kruskal-Wallis H test. Gender data was represented by the frequency of cases, and comparisons across groups were carried out using the chi-squared test. $P < .05$ was considered statistically significant. A one-way ANOVA was employed to analyze the differences among different groups in the functional composite units of neurovascular coupling. Multiple comparison correction was conducted using false discovery rate correction ($P < .01$). ROC curves were utilized to assess the ability of functional composite units in distinguishing between various types of amblyopia. Spearman correlation analysis was conducted between neurovascular coupling in the localized brain area, and BCVA in participants with amblyopia.

To investigate the relationship between the specific receptors/transporters, and the functional composite units of neurovascular coupling, a spatial correlation analysis was performed to examine the concordance between differential brain region maps and the spatial distribution of receptors and transporters. The effect size of diencephalic region maps between different groups was assessed to be spatially correlated with PET/SPECT images using the JuSpace toolbox.[59] The investigation focused on serotonin receptor system (5-HT1a, 5-HT1b, 5-HT2a and SERT), the dopaminergic system (D1, D2, DAT and FDOPA), the noradrenaline transporter (NAT), the GABAergic system (GABAa), and the metabotropic glutamate receptor (mGluR5). Spearman correlation analysis was carried out, based on neuromorphometrics maps, and the results were subjected to spatial correction using permutation statistics, the "*" represented that the correlation was significant ($P < .05$ for permutation, N = 10000 permutations).